Biochimica et Biophysica Acta 1837 (2014) 1973–1980

Contents lists available at ScienceDirect

Biochimica et Biophysica Acta

journal homepage: www.elsevier.com/locate/bbabio

Real-time optical studies of respiratory Complex I turnover ☆

Nikolai Belevich *, Galina Belevich, Marina Verkhovskaya *

Helsinki Bioenergetics Group, Institute of Biotechnology, University of Helsinki, PO Box 65 (Viikinkaari 1), FIN-00014, Finland

ARTICLE INFO

Article history:
Received 24 June 2014
Received in revised form 28 August 2014
Accepted 23 September 2014
Available online 2 October 2014

Keywords:
NADH:ubiquinone oxidoreductase
Proton pump
Electron transfer
Stopped-flow

ABSTRACT

Reduction of Complex I (NADH:ubiquinone oxidoreductase I) from *Escherichia coli* by NADH was investigated optically by means of an ultrafast stopped-flow approach. A locally designed microfluidic stopped-flow apparatus with a low volume (0.2 μl) but a long optical path (10 mm) cuvette allowed measurements in the time range from 270 μs to seconds. The data acquisition system collected spectra in the visible range every 50 μs. Analysis of the obtained time-resolved spectral changes upon the reaction of Complex I with NADH revealed three kinetic components with characteristic times of <270 μs, 0.45–0.9 ms and 3–6 ms, reflecting reduction of different FeS clusters and FMN. The rate of the major (τ = 0.45–0.9 ms) component was slower than predicted by electron transfer theory for the reduction of all FeS clusters in the intraprotein redox chain. This delay of the reaction was explained by retention of NAD^+ in the catalytic site. The fast optical changes in the time range of 0.27–1.5 ms were not altered significantly in the presence of 10-fold excess of NAD^+ over NADH. The data obtained on the NuoF E95Q variant of Complex I shows that the single amino acid replacement in the catalytic site caused a strong decrease of NADH binding and/or the hydride transfer from bound NADH to FMN.

1. Introduction

Respiratory Complex I is an integral membrane protein found both in mitochondria and respiring bacteria, which catalyzes the electron transfer from NADH to ubiquinone, coupled with the translocation of 3 [1] or 4 [2–4] protons across the membrane. In contrast to other complexes of the respiratory chain, where proton pumping mechanisms are understood in principle, the mechanism of Complex I still remains unknown. The enzyme is L-shaped and consists of two domains: the hydrophilic fragment containing FMN and an intraprotein redox chain of FeS clusters, which delivers electrons from NADH to ubiquinone, and the hydrophobic membrane domain containing subunits analogous to monovalent cation/proton antiporters [5], which perform H^+ translocation. The ubiquinone binding site is located on the junction of these domains [6]. No redox centers are found in the membrane fragment where the antiporter-like subunits are disposed in a row so that the energy of the redox reaction must be transduced over a distance of 100 Å. Electron and proton transfers are highly spatially separated as opposed to the case in respiratory complexes III and IV (see for reviews e.g. [7] and [8], respectively), which suggests that Complex I operates by an entirely different mechanism. Strong progress in Complex I studies was achieved by employment of bacterial enzymes that are half the size and have a simpler architecture than the mitochondrial one, while they contain the same core subunits and perform the same basic function. A high resolution 3D structure of bacterial Complex I obtained by X-ray crystallography provided invaluable information on the location of FeS clusters, the ubiquinone binding pocket, and disposition of the H^+ translocation machinery [5,9,10]. However, the static 3D structure cannot be easily interpreted in terms of the molecular mechanism, which requires monitoring the enzyme performance upon turnover in real time. The first attempt of kinetic studies of Complex I reduction was made by Orme-Johnson et al. in 1974 by means of EPR spectroscopy combined with freeze-quenching [11]. They failed to determine the time sequence of reduction of the FeS centers because all the centers were reduced by excess of NADH within 6 ms at 4 ° C, which was the earliest resolved time available with their apparatus. We have studied the electron transfer in Complex I by EPR spectroscopy using a home-made ultra-fast freeze-quench setup with better time resolution. The oxidized enzyme was mixed with NADH and rapidly frozen at particular time intervals. The obtained data indicated that after binding of one NADH molecule the first pair of electrons was transferred simultaneously (an apparent time constant $\tau \approx 100$ μs) to two FeS clusters N1a and N2, which are spatially separated by ~100 Å, both having the highest E_m values among the FeS clusters of the chain. The fast reduction of N1a and N2 was followed by a slow component ($\tau \approx 1$ ms) representing the reduction of the other FeS clusters [12,13]. The observed rate of N2 reduction was very close to the rate expected from electron tunneling theory across the entire span of FeS centers (τ ~ 100 μs [14]); therefore,

Abbreviations: E_h, apparent redox potential; E_m, midpoint redox potential; EPR, electron paramagnetic resonance; ROS, reactive oxygen species

☆ This work is dedicated to the memory of Michael Verkhovsky, whose ideas and studies it is based upon.

* Corresponding authors.
E-mail addresses: Nikolai.Belevich@Helsinki.Fi (N. Belevich), Marina.Verkhovskaya@Helsinki.Fi (M. Verkhovskaya).

http://dx.doi.org/10.1016/j.bbabio.2014.09.010
0005-2728/

this electron transfer is unlikely to be coupled to other reactions, such as proton transfer or conformational changes. Since all elementary rate constants of electron transfer between the clusters were several orders of magnitude higher than this observed rate, we concluded that the reduction of the remaining clusters was limited by a single process, viz. the dissociation of the oxidized NAD^+ molecule from its binding site, where it prevents the entry of the next NADH molecule [12]. However, the freeze-quench approach leaves some uncertainty in the data interpretation due to the theoretic possibility of electron tunneling in frozen protein samples; therefore it is of high importance to monitor Complex I reduction in real-time by an independent technique.

Here we present the first attempts to follow the events in the Complex I catalytic cycle by optical spectroscopy using an ultra-fast microfluidic stopped-flow apparatus. The observed kinetics of Complex I reduction by NADH indicated an essentially biphasic reaction in agreement with our previous EPR data.

2. Materials and methods

2.1. Ultra-fast stopped-flow setup for optical spectroscopy

The most important parameter for the stopped-flow system is its dead time. Most often, a small optical response and low signal to noise ratio in enzymatic studies force researchers to use a cell with a relatively long, 10 mm, optical path that guarantees sufficient sensitivity of the measurements. Conventional stopped-flow systems with a 10 mm light path provide a mixing dead time not better than a few milliseconds. Since enzyme turnover is in most cases faster than 2–3 ms, such systems are not suitable for real time studies of the events in the catalytic cycle. Besides, a standard 10 mm cell requires a rather large sample volume (100–250 μl per one shot), which is another important parameter for the stopped-flow system, because enzyme isolation and purification consume both time and funding. Here, we report the design of a novel microfluidic stopped-flow system that combines a unique low volume flow cell (0.2 μl) with a long optical path (10 mm) thus optimizing both timing and sample consumption characteristics.

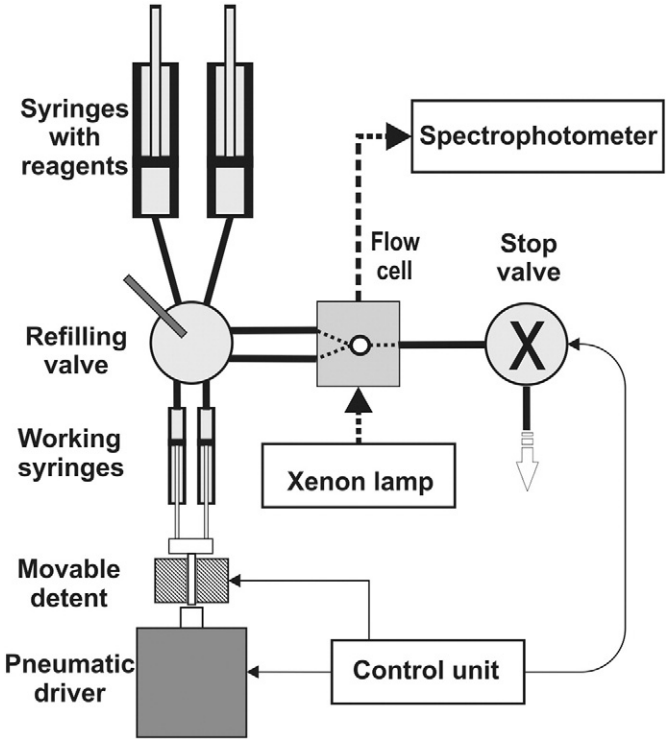

Fig. 1. The simplified diagram of the stopped-flow system.

2.2. Construction of microfluidic stopped-flow apparatus

The simplified diagram of the stopped-flow system is shown in Fig. 1. Syringes with reagents (Hamilton gas tight 1 ml) are connected to the system by means of a refilling valve (Rheodyne 7000) for loading the working syringes with the reagents. Working syringes have a volume of ~80 μl each and are specially designed for high pressure. This volume is enough for several sequential shots (for example 10 shots at 7 μl/shot per syringe). Volume per shot is specified by a movable detent. During the shot the speed of the plungers' progress is measured by the control unit, so that the final flow rate may be monitored. All shots are highly reproducible and a number of sequential shots could be averaged by data acquisition software in order to improve signal to noise ratio. A home-made solenoid valve used as a stop device has a fast response, within several milliseconds, and a low inner volume. The design of the valve could be simply described as a spring-loaded plug, which closes a hole with the diameter of 250 μm. The stop valve is synchronized with the syringe driver and its delay may be adjusted with high precision. All components in the flow path are connected by stainless steel tubes with an inner diameter of 250 μm. A 150 W xenon lamp is used as the light source. A fast spectrophotometer, which is built on the base of the spectrograph CP-140 (Jobin Yvon), equipped by a fast line scan CMOS camera spL2048-140 km (Basler Vision Technologies), is capable of acquiring up to 140 spectra per 1 ms. The light source, the flow cell, and the spectrophotometer, are coupled by fiber optics.

2.3. Design of the flow cell

The body of the flow cell was made of stainless steel and has a cylindrical shape with 6 mm in diameter and 10 mm length. The round channel along the cylinder axis serves as the optical part of the cell. The channel has a diameter of ~150 μm and the length of 10 mm. The inner volume of the channel is below 0.2 μl. The inner surface of the channel is polished in order to decrease light loss. Input and output tubes connected to the cell body create a Z-type shape of the flow cell (Fig. 2). A turbulent alcove-based mixer is located on the flat surface of the cell body near the entrance to the optical part. The design of the mixer is based on ideas described in [15]. In this mixer, the two reagents to be mixed meet at the central "T" junction, where they are directed into a channel with the three alcoves, each with a triangular obstruction, arranged in a zigzag fashion. A chaotic flow due to recirculation within the alcoves results in transverse velocity that promotes effective fluid mixing at a relatively low Reynolds number.

The mixer was fabricated using electrochemical micromachining technology according to [16–18]. In this technology application of ultra-short voltage pulses to a tiny tool electrode under suitable electrochemical conditions enables precise machining of stainless steel. Mixer channels have a depth 200 μm and a width in the range of 30–50 μm (Fig. 2). The flow cell is assembled in the cell holder where two quartz windows close the flat surfaces of the cell body on both sides. The cell holder includes collimating lenses and SMA connectors to couple with fiber optics. Upon the shot the flow rate inside the chamber is ~500 μl/s. At this flow rate flux could be characterized as turbulent with Reynolds number above 4000.

During the data acquisition we observed a signal distortion at the moment when the stop valve closes the flow path. This distortion could be explained by several factors. First, the light passing through the optical cell undergoes multiple reflections from the channel wall since the length to diameter ratio is about 66. The optical behavior of the thin layer of liquid, adjacent to the channel wall, could be responsible for the distortion as well as a turbulent/laminar transition of the flow. Second, the liquid contains dissolved gases and a cavitation effect could occur due to the pressure jump upon closing the valve. However, this distortion is highly reproducible and can be subtracted using the reference data set, obtained for example by mixing water with water.

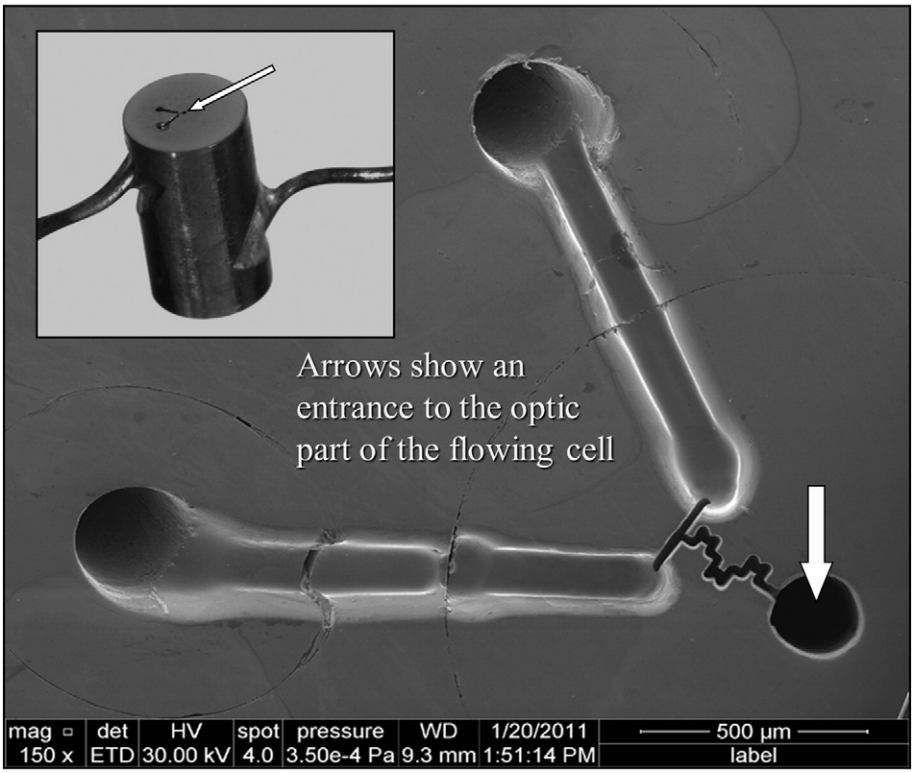

Fig. 2. ESM image of the alcove-based mixer, fabricated on the flat surface of the cell body. The mixer has channels with depths of 200 µm and width in range of 30–50 µm. Inset: the overall view of the cell body. Arrows show an entrance to the optical part of the cell.

2.4. Calibration of the microfluidic stopped-flow setup

The interpretation of stopped-flow data requires careful calibration of the instrument. A common test reaction for the fast changes of absorption is the reduction of 2,6-dichlorophenolindophenol (DCIP) by ascorbic acid accompanied by a decrease of DCIP absorbance [19,20]. In this test we could explore a pseudo-first-order reaction as a single-exponential process. Fig. 3 presents series of DCIP absorbance measurements at several ascorbic acid concentrations used for calculation of the dead time of the stopped-flow system. The reaction was started by mixing equal volumes of DCIP (0.125 mM in water) and ascorbic acid at concentrations 2, 10, and 50 mM. Absorbance changes were measured at 525 nm, near the isosbestic point between the acidic and the basic form of DCIP, with the reference at 770 nm where reactants do not absorb; the difference was plotted against the time. After the flow comes to a full stop, the exponential absorbance (signal) decays are observed with rate constants of about 44, 265, and 1360 s^{-1} at final concentrations of ascorbic acid of 1, 5, and 25 mM, respectively. The start of the reaction can be found by the intersection of the exponential fits at an absorbance value $A_0 = 0.463$, which corresponds to the level of the oxidized DCIP before the beginning of the reaction. The dead time can be calculated from the absorbance value in the continuous-flow regime prior to closure of the stop valve, A_{cf}, using the following equation:

$$t_{cf} = -\ln(A_{cf}/A_0)/k$$

where A_0 is the absorbance of DCIP before the start of the reaction and k is the first-order rate constant obtained by exponential fitting. In our case we have t_{cf} in the range of 0.26–0.27 ms that characterizes the dead time for the mixer and the flow cell. However, t_{cf} does not account for the finite stop time and stop-related artifacts. The delay between the intercept of the fits and the first data point that joins the fitted exponential provides an estimate of the instrumental dead time (Fig. 3); the experimental data that could be fitted as a kinetics can be obtained only from ~0.36 ms. From these data it could be concluded that our stopped-flow cell has good mixing properties, however, the stop valve is not capable to stop the flow instantly. During the stop event the flux inside the cell undergoes transition: turbulent → laminar → full stop which results in a loss of almost 100 µs of the reaction time. Finally, for the particular kinetics we

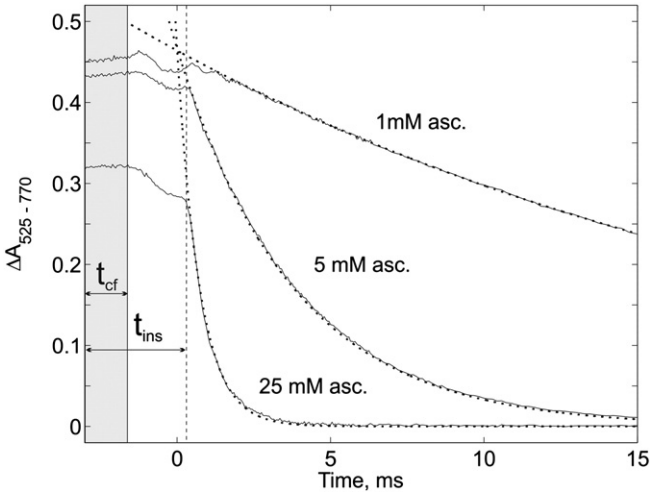

Fig. 3. Determination of the dead time of the microfluidic stopped-flow system using the reduction of DCIP by ascorbic acid as a test reaction. DCIP in water (125 µM) and ascorbic acid at concentrations 2, 10, and 50 mM were mixed at a total flow rate 0.5 ml/s with 1:1 ratio. Each trace represents the averaged data set, obtained from 10 sequential shots. Dotted lines show fitted exponents with the rate constants of 44 s^{-1}, 265 s^{-1} and 1360 s^{-1} at final concentration of ascorbic acid 1, 5 and 25 mM, respectively. The shaded zone corresponds to a constant flow regime with dead time $t_{cf} = 0.26$–0.27 ms. Vertical dashed line indicates the limit of the instrument dead time t_{ins} ~0.36 ms and represents the full stop of the flux. Zero time on the x-axis corresponds to the beginning of the DCIP reduction.

have a single averaged spectrum obtained at reaction time 0.27 ms (dead time) and continuous kinetic data starting at 0.36 ms. Note that time values before zero on the X-axis have no numerical meaning considering the chemical reaction. Physical time of the constant flow regime could be as long as needed for obtaining good quality spectrum, the time of the reaction is the same and determined as described (0.27 ms).

3. Bacterial growth and purification of Complex I

The *Escherichia coli* MWC215 (Sm^R *ndh*::Cm^R) strain was grown in LB medium at 37 °C and harvested at the late exponential growth phase. The membranes for Complex I purification were prepared by passing the cells through an APV Gaulin homogenizer as described in [21]. Complex I was purified in three chromatography steps, using two anion exchanger DEAE-Trisacryl M (Bio-Sepra) columns and gel filtration on Superdex 200 prep grade (GE Healthcare) [22].

4. Stopped-flow experiments

Purified Complex I (3–6 μM) in buffer containing 100 mM MOPS/KOH, pH 7.0, was mixed with an equal volume of the same buffer with or without of 200 μM NADH (unless differently indicated) and the spectra were collected during 1 s.

The acquired with 50 μs resolution spectra were logarithmically averaged: in the beginning of the kinetics each 50 μs spectrum was taken in, and in the end the distance between data points increased up to 20 ms (approximately 300 spectra were averaged). All collected spectra were combined to form a data surface.

For each matrix the data of 40–50 single shots (7 μl per shot) were averaged. The difference obtained between these two matrices presents the kinetics of Complex I reduction (a set of Complex I redox spectra). NADH absorption spectra were subtracted. All the experiments were conducted at room temperature.

5. Data analysis

Basic data matrix manipulations and analysis were carried out with MATLAB (the Mathworks, Inc.). Decomposition of the kinetic data surfaces was achieved by global fitting run under a MATLAB interface using the Rakowsky algorithm as described in [23]. The fitting was performed using kinetic points starting from 360 μs, dead time spectrum, 270 μs (see calibration, Fig. 3) and zero time spectrum obtained from the oxidized Complex I by the same setup.

6. Results

Complex I reduction by NADH was followed by means of the ultrafast microfluidic stopped flow apparatus in the time range from 270 μs to 1 s. Spectra derived from FeS clusters and FMN were obtained. The raw data are shown in Fig. 4A as the set of redox spectra. Fig. 4B shows the individual spectra at 270 μs (so called dead time spectrum) and at 10 ms when the reaction was completed. The kinetics taken at a particular wavelength from 410 to 460 nm cannot be fitted with only one component; the fit can be obtained by contribution of three phases (Fig. 5A). The global fitting of the whole matrix also showed three components (Fig. 5B) indicating that particular FeS clusters are reduced at different time intervals. The characteristic time of the fastest phase falls into the time interval ($\tau_1 = 60 \div 120$ μs) which is below the dead time of the setup and cannot be well determined. The characteristic time of the second phase is below 1 ms, ($\tau_2 = 450$–900 μs); the third and slowest phase takes several milliseconds ($\tau_3 = 3$–6 ms).

The NADH absorption spectrum overlaps with that of Complex I at the blue end; a high NADH concentration makes it difficult to determine the correct shape of the Complex I spectrum below 400 nm. Therefore, a low NADH concentration is preferable, but the rate of the whole

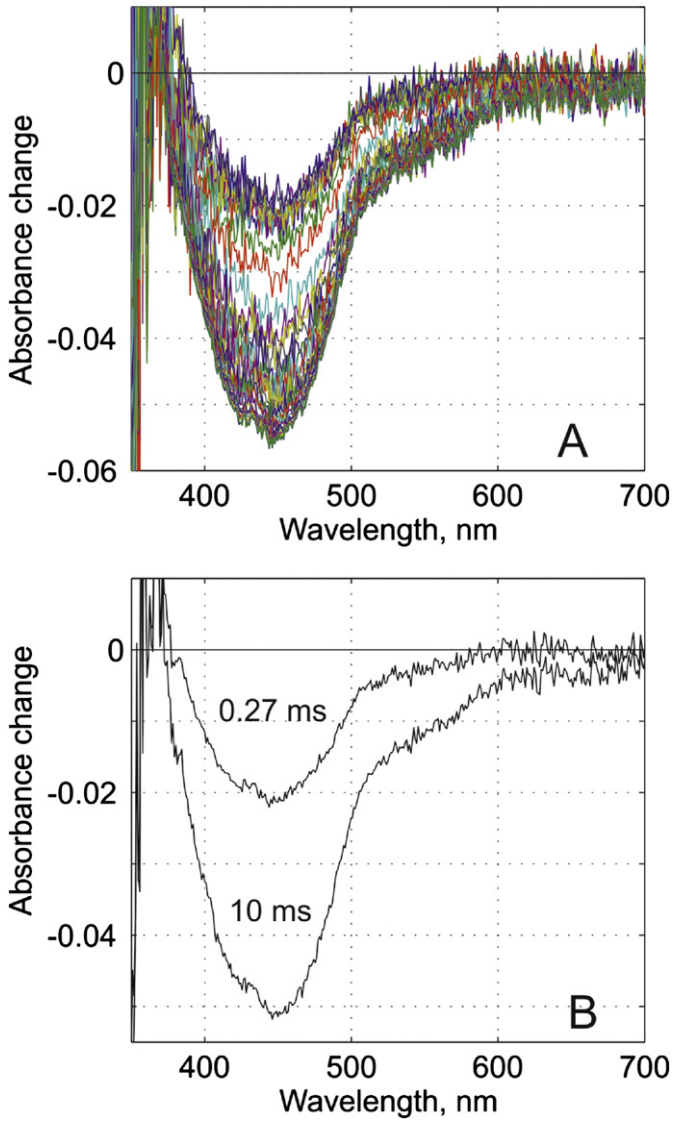

Fig. 4. Time-resolved reduction of Complex I by NADH. A. The set of redox spectra obtained after mixing of 6 μM Complex I with 200 μM NADH at a time range from 270 μs to 1 s. B. Redox spectra of Complex I at 270 μs (dead time spectrum) and at 10 ms (the reaction completed).

reaction must not be limited by NADH binding. Previously the bimolecular rate constant was determined to be $8.3 \times 10^7\ M^{-1}\ s^{-1}$ [12], which in our conditions yields NADH binding in ~100 μs, which is within the dead time of the apparatus.

If the reaction is constrained by NADH concentration the amplitude of the fastest optical phase should decrease relative to the amplitude of fully reduced Complex I and the kinetics of the second phase could be slower. Indeed, the dead time spectrum upon mixing Complex I with 20 μM NADH was less than half the amplitude upon mixing with 100 and 200 μM NADH (Fig. 6A). The kinetics of the second phase upon mixing Complex I with 20 μM NADH was slower and the amplitude was less (Fig. 6B). It is difficult to analyze such kinetics properly because the concentration of NADH was not constant upon measurements: immediately after mixing it dropped below K_m (10 μM for Complex I from *E. coli* [24]), after several milliseconds the ratio NADH/NAD^+ strongly decreased and the enzyme was equilibrated thermodynamically. Surprisingly, the dependence of the dead time spectrum amplitude on NADH concentration was observed at rather low NADH concentration: an abrupt amplitude drop occurred when the NADH concentration after mixing was 30 μM (Fig. 6B, inset). This means that the previously

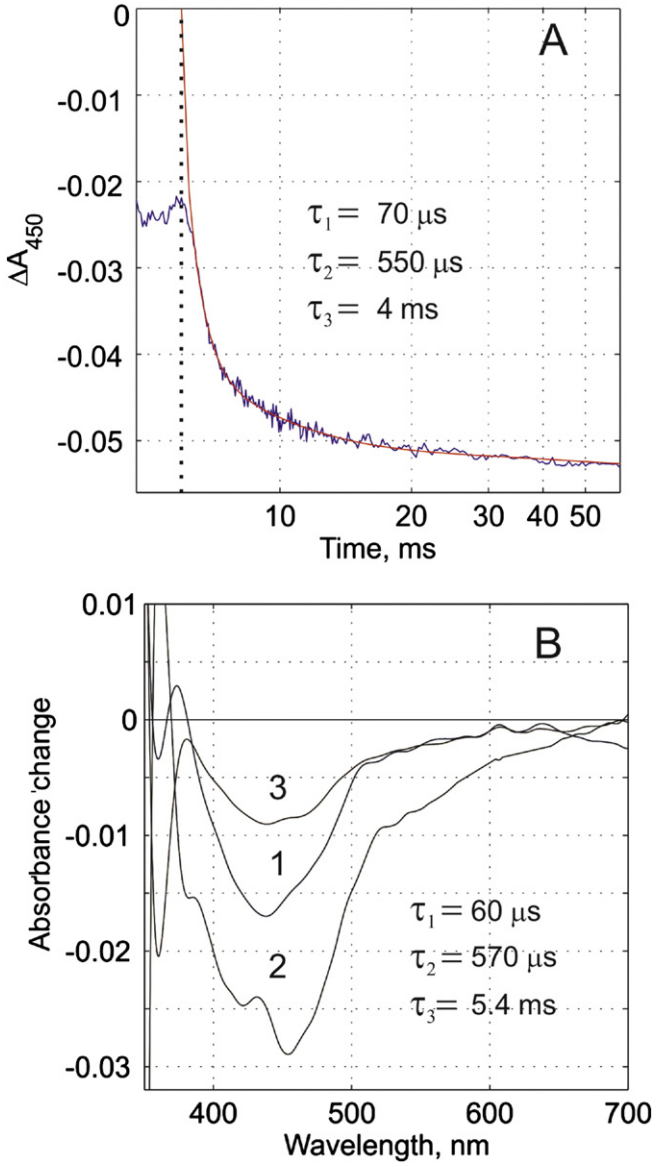

Fig. 5. The kinetic parameters of Complex I reduction. A. The kinetics of Complex I reduction at 450 nm. The dotted line indicates the start of the reaction. The amplitude of optical changes before the dotted line reflects the events occurring during the dead time (270 μs). The kinetics was fitted by the sum of three exponents (red line) with shown characteristic times. B. Spectral components obtained by global fitting of the experimental kinetic data; characteristic times are indicated. Characteristic times varied in different experiments in the range $\tau_1 = 60 \div 120$ μs, $\tau_2 = 450 \div 900$ μs, $\tau_3 = 3 \div 6$ ms.

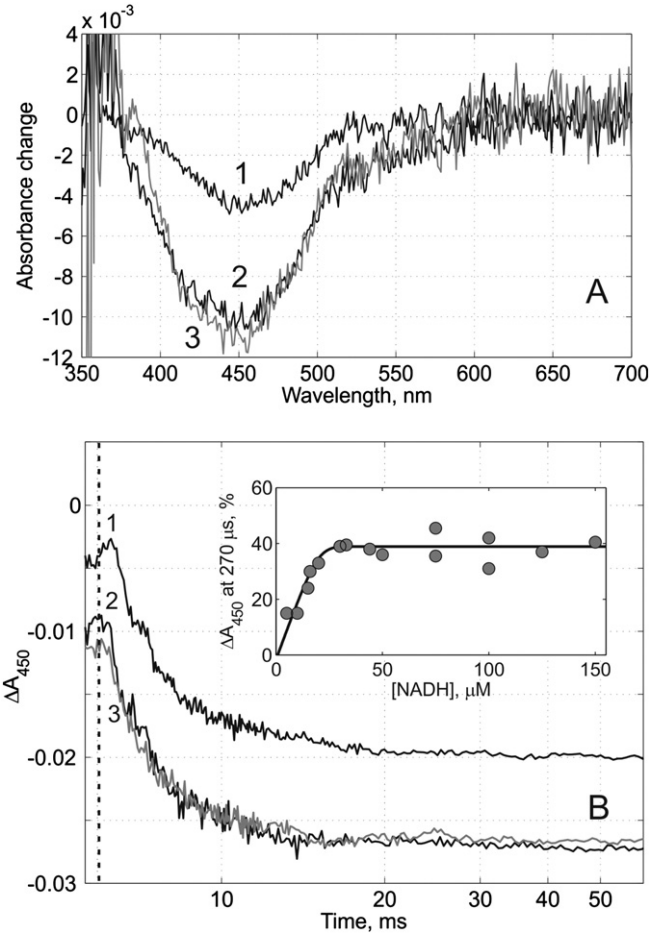

Fig. 6. Dependence of the Complex I reduction kinetics on NADH concentration. A. Dead time (270 μs) spectra upon mixing Complex I with NADH at concentration 20 μM, curve 1, 100 μM, curve 2, and 200 μM, curve 3. B. Kinetics of Complex I reduction at 450 nm upon mixing with NADH at concentration 20 μM, curve 1, 100 μM, curve 2 and 200 μM, curve 3. Inset: dependence of the ratio of amplitudes of dead time spectrum and spectrum of fully reduced Complex I on NADH concentration after mixing.

determined bimolecular rate constant was underestimated to some extent, the difference could be due to a difference in the measurement conditions.

To test how NAD^+ affects the fast reduction of Complex I, the enzyme was mixed with the buffer containing 220 μM NADH and 2.2 mM NAD^+. The fastest phase of the reaction was almost identical to that in the absence of NAD^+ (Fig. 7). The dead time spectra in the presence and absence of NAD^+ differ insignificantly (Fig. 7, inset). Although the beginning of the kinetics looks similar, it is impossible to fit the curve in the presence of NAD^+: the reduction stops at 4–5 ms due to thermodynamic equilibration of the enzyme with an ambient E_h of −290 mV.

Completely different kinetics were observed upon reduction of the mutated Complex I bearing the replacement of the invariant Glu95 with glutamine in the nucleotide- and FMN-binding subunit NuoF. Glu95 is located in the vicinity of FMN and participates in the formation of the cavity where the NADH (and NAD^+) nicotinamide ring binds. Studies of the properties of the E95Q variant in steady-state and equilibrium conditions indicated moderate changes in the nucleotide affinity,

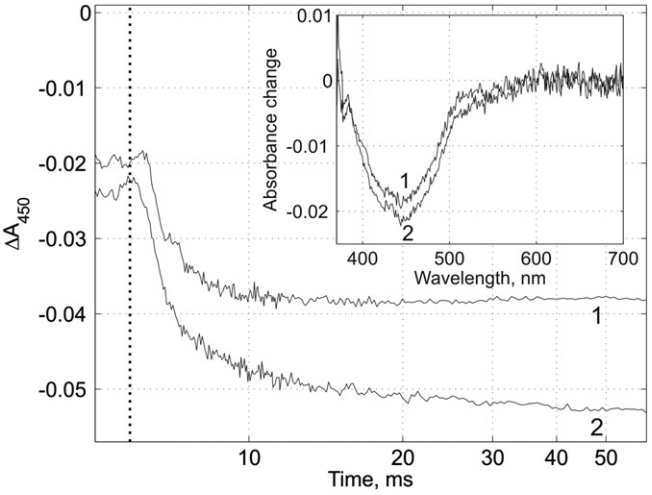

Fig. 7. Effect of NAD^+ on the fast Complex I reduction. Kinetics at 450 nm in the presence of 2.2 mM NAD^+, curve 1, and in its absence, curve 2. NADH concentration 220 μM. Inset: dead time spectra in the presence of NAD^+, curve 1, and in its absence, curve 2.

but a significant positive shift of the midpoint redox potential of FMN [24]. Later we have found that such replacement results in a massive electron leakage from the catalytic site [25]. Monitoring the kinetics of E95Q reduction showed almost complete lack of the fastest first phase of the reaction (Fig. 8A), i.e. practically no dead time spectrum was observed.

Decomposition of the kinetic data surface by global fitting results in essentially two phases (the first, fastest phase was negligible), both of which were much slower than those in the wild type (Fig. 8B). The phase with largest amplitude, $\tau_2 = 5$–6 ms, did not show any particular spectral features in contrast to wild type enzyme. The slowest phase was also significantly slower than in wild type, $\tau_3 = 700$ ms, and it had more absorption in the blue end.

7. Discussion

Our time-resolved spectroscopic kinetic studies using the ultrafast microfluidic stopped flow apparatus indicated that the reduction of Complex I by excess of NADH can be decomposed into three phases. The initial events in the enzyme catalytic turnover are NADH binding and sequential oxidoreduction of FMN and certain FeS centers. Obviously, FMN reduction is a very fast transient event: as soon as it is reduced by NADH it should be oxidized within 0.5 μs by the two FeS centers nearby [26]. Therefore, this transition cannot contribute to the spectrum obtained in the dead time of our setup (270 μs). If the presented data are juxtaposed with the results obtained by fast EPR spectroscopy measurements [12], the suggestion can be made that a significant part of the dead time spectrum and the spectrum of the first component obtained by global fitting (Fig. 5B), comprises the spectra of the two clusters with the highest midpoint redox potentials, N1a and N2, which were reduced with $\tau \approx 100$ μs. The other FeS clusters of the chain also could contribute to some extent since some portion of the second phase proceeds during the dead time (0.27 ms). The second resolved phase is due to reduction of the rest of the FeS clusters and probably partial reduction of FMN. The characteristic time of this phase ($\tau_2 =$ 450–900 μs) is just slightly shorter than that determined by treatment of the EPR data ($\tau_2 \approx 1000$ μs). However, the reaction resolved optically as the slowest third phase with small amplitude (Fig. 5B) could contribute to the previous EPR measurements: the two slowest phases could be merged upon treatment of the EPR data. Thus, the results of the fast optical measurements are in agreement with the data obtained by EPR spectroscopy: both approaches clearly show that the rate of reduction of the majority of the FeS clusters is obviously slower than has been predicted by electron transfer theory [14]. This phenomenon could be explained by slow dissociation of the oxidized substrate (NAD^+) molecule from the binding site, which would decrease the reaction rate (becomes the rate-limiting step) as we suggested previously [12]. The other possible reason for this retardation can be found considering intraprotein electrostatic interactions [27–31]. According to Stuchebrukhov and coauthors, the electron tunneling between two pairs of clusters, namely N3 → N1b and N5 → N6a, is drastically slower than predicted earlier, unless structural water is included. Only on this condition is the overall transfer rate roughly equal to a typical electron transfer rate for such a distance. These authors suggested that intervening water molecules are not seen in the structure of the hydrophilic domain of Complex I due to their possible significant mobility. It can be assumed that there could be "dry"/"watered" protein transitions or intermediate states resulting in slackened electron transfer. However, if the breakpoint occurs in the intraprotein FeS chain, the prominent spectrum of reduced FMN should be observed in the millisecond time range which was not the case. Moreover, the fast reduction of center N2 by NADH observed here and in the earlier EPR study contradicts such a block in electron transfer. However, the electrostatic interactions between low-potential FeS clusters could be a reason for the third, slowest phase of Complex I reduction, when the enzyme is loaded with electrons due to multiple NADH oxidation.

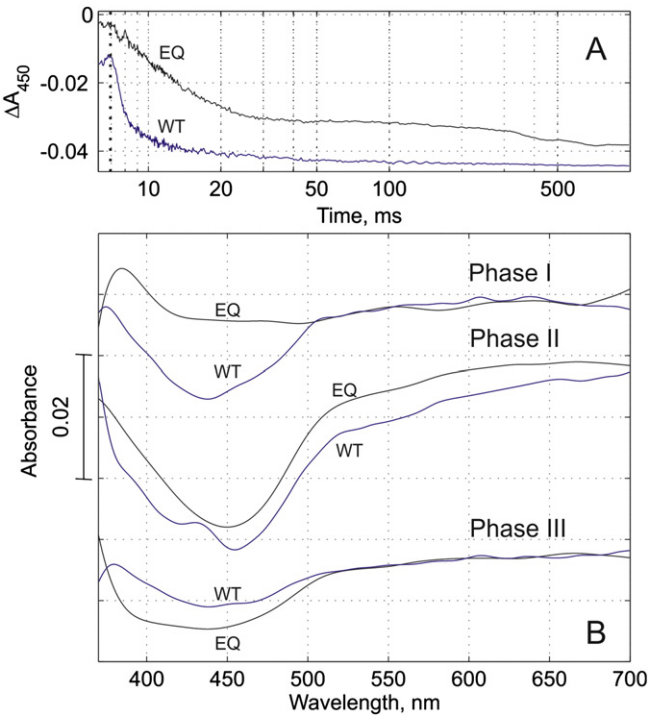

Fig. 8. Reduction of NuoF E95Q variant (EQ) by NADH in comparison with wild type (WT). A. The kinetics of Complex I reduction at 450 nm. The dotted line indicates the start of the reaction. B. Spectral components were obtained by global fitting of the experimental kinetics.

Thus, the most plausible cause of the delay in Complex I reduction is the retention of NAD^+ in the catalytic site which may be physiologically important. Previously we have found that the delivery of two electrons from the first NADH molecule bound to Complex I did not result in semiquinone formation or ubiquinone reduction although the enzyme contains one molecule of tightly bound ubiquinone. The two first electrons were distributed between two FeS clusters with the highest midpoint redox potentials which led us to the conclusion that bound semiquinone has a very low E_m and that only delivery of the second electron to ubiquinone is coupled to a large potential drop that drives the translocation of all four protons across the membrane [12]. The life-time extension of the two-electron state of Complex I caused by slow NAD^+ release may be required to initiate a conformational change that activates the proton pumping machinery and/or for diffusion of a pool ubiquinone. In other words this state could be necessary to keep the enzyme ready for immediate operation when the next NADH molecule is bound. Hence, the excessive loading of the intraprotein redox chain with electrons, which could result in ROS production and delayed electron transfer, would be prevented.

Studying the kinetics of Complex I reduction under conditions of 10-fold excess of NAD^+ over NADH did not show a significant delay of the fast reaction. At a first glance, this conflicts with the suggestion of slow release of NAD^+ after NADH oxidation. This seeming contradiction may be resolved by the assumption of high selectivity of the entrance to the catalytic site. The major difference between the two nucleotides is a positive charge on the nitrogen of the nicotinamide ring of NAD^+. Although both nucleotides are negatively charged overall, one can speculate that the selection is based on the electrostatic interactions and spatial constrains. A positively charged amino acid residue sitting at the entrance of the deep cavity, on the bottom of which FMN is partially buried, may repulse NAD^+ upon its diffusion to and from the catalytic site through the narrow

input. Conserved Lys202 and Lys75 (*Thermus thermophilus* nomenclature) in the catalytic NuoF subunit could be good candidates for such a "gate keeper" role as shown in Fig. 9. Analysis of the 3D structure of the catalytic site made Berrisford and Sazanov to conclude that Lys202 and Lys75 make H-bonds with the oxygen of pyrophosphate and adenosine ribose, respectively, upon nucleotide binding [32] which does not hinder its preceding electrostatic interaction with the positively charged nicotinamide ring upon NAD^+ penetration into the FMN containing cavity. As soon as the nicotinamide of NAD^+ approaches its proper position, relatively near the FMN alloxazine, the lysines at the entrance do not affect the nucleotide binding but they would delay its diffusion. Such enzyme design would not change the affinity of the catalytic site but it could significantly decrease the on- and off-rate constants.

It is also possible that the binding characteristics of Complex I may depend on the direction of the electron flux providing the drastic difference in the apparent affinity to NAD^+ upon forward and reverse electron transport (forward reaction: K_i^{NAD+} is close to 1 mM [24,33], reverse reaction: K_m^{NAD+} is 7 μM [34,35]) as was proposed by Grivennikova et al. [36] and Sazanov [37]. The distinction between the forward and reverse reactions is that the intraprotein redox chain is partially oxidized upon the former, whereas the FeS clusters and, consequently, FMN are reduced upon the latter. Negatively charged FMN should attract NAD^+ and/or neutralize the effect of the positively charged gate keeper and therefore abolish the diffusion obstacle. That does not concern the neutral NADH molecule and, obviously, its on–off-rate constants are not dependent on the direction of the electron flux.

The single replacement, E95Q, in the catalytic site of Complex I drastically changes the whole reaction. The fastest phase was almost eliminated, which suggests a large decrease of the NADH binding constant and/or retardation of the hydride transfer from NADH to FMN due to some distortion of the catalytic site. The determined K_m^{NADH} values for the E95Q variant and wild type enzyme are very close [24] which makes the second assumption more probable. The second and the third phase were also decelerated and that could be explained by the previously found massive electron leakage from the catalytic site in the E95Q variant [25].

Finally, our initial results with the newly designed microfluidic stopped-flow apparatus clearly show that it is highly beneficial for mechanistic studies of the enzymes by optical methodology, due to its fast operation and its sensitivity to small absorption changes.

Acknowledgements

This work was supported by grants from the Biocentrum Helsinki (grant 7919530), the Sigrid Juselius Foundation (grant 4702217), and the Academy of Finland (grant 132779). The authors are grateful

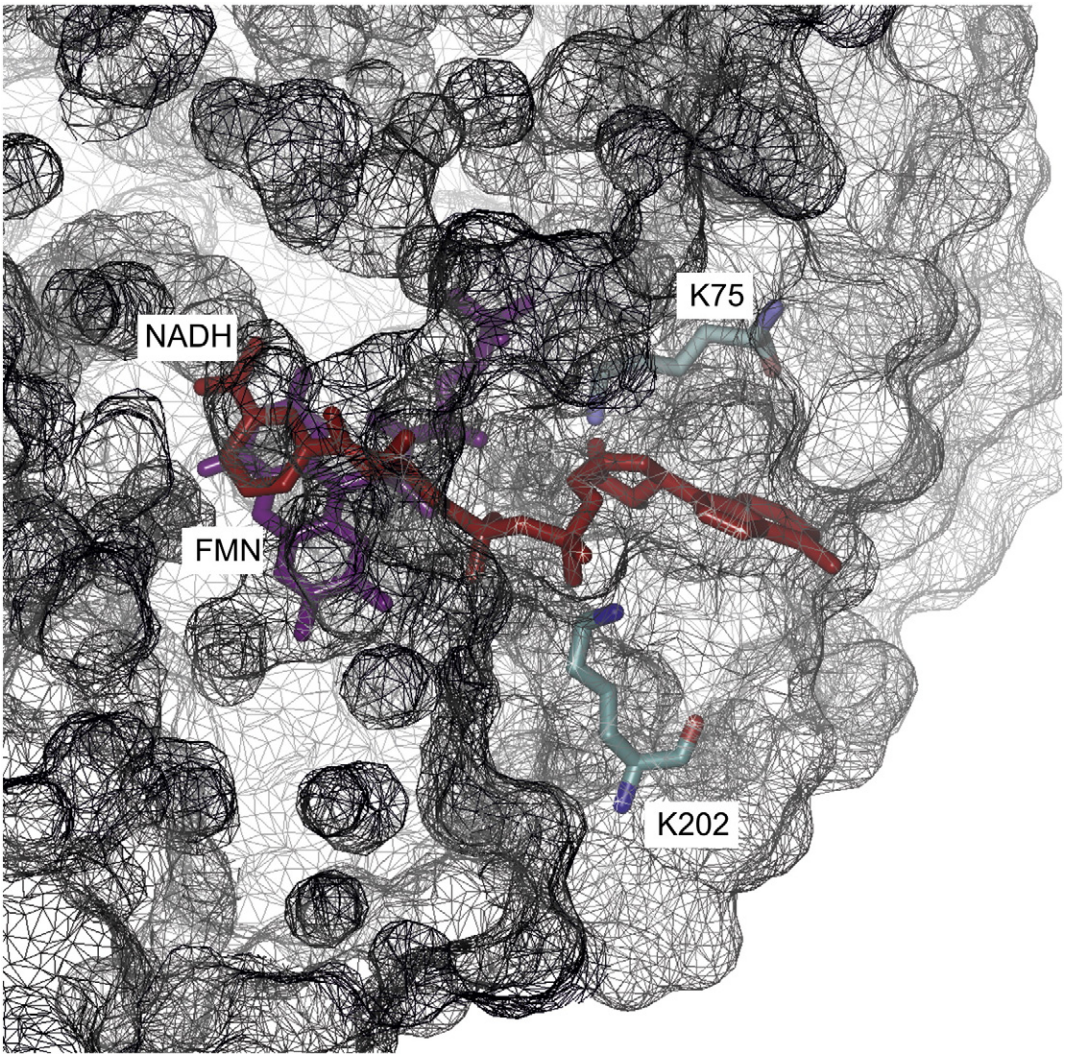

Fig. 9. Catalytic site of Complex I of *T. thermophilus* (PDB ID: 3IAM). FMN and NADH are located at the bottom of the cavity in the catalytic subunit. Lysines 202 and 75 are positioned at the entrance of the cavity.

to Dr. Mårten Wikström for critical reading the manuscript and valuable comments. We thank Eija Haasanen for purification of Complex I. The authors are grateful to Dr. Alexander Bogachev for many inspiring and stimulating discussions.

References

[1] M. Wikström, G. Hummer, Stoichiometry of proton translocation by respiratory complex I and its mechanistic implications, Proc. Natl. Acad. Sci. U. S. A. 109 (2012) 4431-4426.
[2] P.C. Hinkle, M.A. Kumar, A. Resetar, D.L. Harris, Mechanistic stoichiometry of mitochondrial oxidative phosphorylation, Biochemistry 30 (1991) 3576–3582.
[3] M. Wikström, Two protons are pumped from the mitochondrial matrix per electron transferred between NADH and ubiquinone, FEBS Lett. 169 (1984) 300–304.
[4] A.S. Galkin, V.G. Grivennikova, A.D. Vinogradov, $H^+/2e^-$ stoichiometry in NADH–quinone reductase reactions catalyzed by bovine heart submitochondrial particles, FEBS Lett. 451 (1999) 157–161.
[5] R.G. Efremov, R. Baradaran, L.A. Sazanov, The architecture of respiratory complex I, Nature 465 (2010) 441–445.
[6] R. Baradaran, J.M. Berrisford, G.S. Minhas, L.A. Sazanov, Crystal structure of the entire respiratory complex I, Nature 494 (2013) 443–448.
[7] A.R. Crofts, The cytochrome bc1 complex: function in the context of structure, Ann. Rev. Physiol. 66 (2004) 689–733.
[8] I. Belevich, M.I. Verkhovsky, Molecular mechanism of proton translocation by cytochrome c oxidase, Antioxid. Redox Signal. 10 (2008) 1–29.
[9] R.G. Efremov, L.A. Sazanov, Structure of the membrane domain of respiratory complex I, Nature 476 (2011) 414–420.
[10] R.G. Efremov, L.A. Sazanov, The coupling mechanism of respiratory complex I — a structural and evolutionary perspective, Biochim. Biophys. Acta 1817 (2012) 1785–1795.
[11] N.R. Orme-Johnson, R.E. Hansen, H. Beinert, Electron paramagnetic resonance-detectable electron acceptors in beef heart mitochondria. Reduced diphosphopyridine nucleotide ubiquinone reductase segment of the electron transfer system, J. Biol. Chem. 249 (1974) 1922–1927.
[12] M.L. Verkhovskaya, N. Belevich, L. Euro, M. Wikström, M.I. Verkhovsky, Real-time electron transfer in respiratory complex I, Proc. Natl. Acad. Sci. U. S. A. 105 (2008) 3763–3767.
[13] N.P. Belevich, M.L. Verkhovskaya, M.I. Verkhovsky, Chapter 4. Electron transfer in respiratory complexes resolved by an ultra-fast freeze-quench approach, Methods Enzymol. 456 (2009) 75–93.
[14] C.C. Moser, T.A. Farid, S.E. Chobot, P.L. Dutton, Electron tunneling chains of mitochondria, Biochim. Biophys. Acta 1757 (2006) 1096–1109.
[15] T. Egawa, J.L. Durand, E.Y. Hayden, D.L. Rousseau, S.R. Yeh, Design and evaluation of a passive alcove-based microfluidic mixer, Anal. Chem. 81 (2009) 1622–1627.
[16] R. Schuster, V. Kirchner, P. Allongue, G. Ertl, Electrochemical micromachining, Science 289 (2000) 98–101.
[17] L. Cagnon, V. Kirchner, M. Kock, R. Schuster, G. Ertl, W.T. Gmelin, H. Kuck, Electrochemical micromachining of stainless steel by ultrashort voltage pulses, Z. Phys. Chem. 217 (2003) 299–313.
[18] B.H. Kim, C.W. Na, Y.S. Lee, D.K. Choi, C.N. Chu, Micro electrochemical machining of 3D micro structure using dilute sulfuric acid, CIRP Ann. Manuf. Technol. 54 (2005) 191–194.
[19] B. Tonomura, H. Nakatani, M. Ohnishi, J. Yamaguchiito, K. Hiromi, Test reactions for a stopped-flow apparatus — reduction of 2,6-dichlorophenolindophenol and potassium ferricyanide by L-ascorbic-acid, Anal. Biochem. 84 (1978) 370–383.
[20] H. Roder, K. Maki, H. Cheng, M.C. Shastry, Rapid mixing methods for exploring the kinetics of protein folding, Methods 34 (2004) 15–27.
[21] G. Belevich, L. Euro, M. Wikström, M. Verkhovskaya, Role of the conserved arginine 274 and histidine 224 and 228 residues in the NuoCD subunit of complex I from *Escherichia coli*, Biochemistry 46 (2007) 526–533.
[22] G. Belevich, J. Knuuti, M.I. Verkhovsky, M. Wikström, M. Verkhovskaya, Probing the mechanistic role of the long alpha-helix in subunit L of respiratory Complex I from *Escherichia coli* by site-directed mutagenesis, Mol. Microbiol. 82 (2011) 1086–1095.
[23] D.A. Bloch, A. Jasaitis, M.I. Verkhovsky, Elevated proton leak of the intermediate OH in cytochrome c oxidase, Biophys. J. 96 (2009) 4733–4742.
[24] L. Euro, G. Belevich, D.A. Bloch, M.I. Verkhovsky, M. Wikström, M. Verkhovskaya, The role of the invariant glutamate 95 in the catalytic site of Complex I from *Escherichia coli*, Biochim. Biophys. Acta 1787 (2009) 68–73.
[25] J. Knuuti, G. Belevich, V. Sharma, D.A. Bloch, M. Verkhovskaya, A single amino acid residue controls ROS production in the respiratory Complex I from *Escherichia coli*, Mol. Microbiol. 90 (2013) 1190–1200.
[26] M. Verkhovskaya, D.A. Bloch, Energy-converting respiratory Complex I: on the way to the molecular mechanism of the proton pump, Int. J. Biochem. Cell Biol. 45 (2013) 491–511.
[27] E.S. Medvedev, V.A. Couch, A.A. Stuchebrukhov, Determination of the intrinsic redox potentials of FeS centers of respiratory complex I from experimental titration curves, Biochim. Biophys. Acta 1797 (2010) 1665–1671.
[28] T. Hayashi, A.A. Stuchebrukhov, Electron tunneling in respiratory complex I, Proc. Natl. Acad. Sci. U. S. A. 107 (2010) 19157–19162.
[29] T. Hayashi, A.A. Stuchebrukhov, Quantum electron tunneling in respiratory complex I, J. Phys. Chem. B 115 (2011) 5354–5364.
[30] L. Euro, D.A. Bloch, M. Wikström, M.I. Verkhovsky, M. Verkhovskaya, Electrostatic interactions between FeS clusters in NADH:ubiquinone oxidoreductase (Complex I) from *Escherichia coli*, Biochemistry 47 (2008) 3185–3193.
[31] H.R. Bridges, E. Bill, J. Hirst, Mössbauer spectroscopy on respiratory complex I: the iron–sulfur cluster ensemble in the NADH-reduced enzyme is partially oxidized, Biochemistry 51 (2012) 149–158.
[32] J.M. Berrisford, L.A. Sazanov, Structural basis for the mechanism of respiratory complex I, J. Biol. Chem. 284 (2009) 29773–29783.
[33] T.V. Zharova, A.D. Vinogradov, A competitive inhibition of the mitochondrial NADH–ubiquinone oxidoreductase (complex I) by ADP-ribose, Biochim. Biophys. Acta 1320 (1997) 256–264.
[34] V.G. Grivennikova, R. Roth, N.V. Zakharova, C. Hägerhäll, A.D. Vinogradov, The mitochondrial and prokaryotic proton-translocating NADH:ubiquinone oxidoreductases: similarities and dissimilarities of the quinone-junction sites, Biochim. Biophys. Acta 1607 (2003) 79–90.
[35] A.B. Kotlyar, N. Borovok, NADH oxidation and NAD^+ reduction catalysed by tightly coupled inside-out vesicles from *Paracoccus denitrificans*, Eur. J. Biochem. 269 (2002) 4020–4024.
[36] V.G. Grivennikova, A.B. Kotlyar, J.S. Karliner, G. Cecchini, A.D. Vinogradov, Redox-dependent change of nucleotide affinity to the active site of the mammalian complex I, Biochemistry 46 (2007) 10971–10978.
[37] L.A. Sazanov, Respiratory complex I: mechanistic and structural insights provided by the crystal structure of the hydrophilic domain, Biochemistry 46 (2007) 2275–2288.